Journal of Photonics for Energy

PhotonicsforEnergy.SPIEDigitalLibrary.org

Analysis of luminescence coupling effect in three-terminal tandem solar cells

Takeshi Tayagaki
Kikuo Makita
Ryuji Oshima
Hidenori Mizuno
Takeyoshi Sugaya

SPIE.

Takeshi Tayagaki, Kikuo Makita, Ryuji Oshima, Hidenori Mizuno, Takeyoshi Sugaya, "Analysis of luminescence coupling effect in three-terminal tandem solar cells," *J. Photon. Energy* **8**(4), 045503 (2018), doi: 10.1117/1.JPE.8.045503.

Analysis of luminescence coupling effect in three-terminal tandem solar cells

Takeshi Tayagaki,[a,*] Kikuo Makita,[a] Ryuji Oshima,[a] Hidenori Mizuno,[b] and Takeyoshi Sugaya[a]

[a]National Institute of Advanced Industrial Science and Technology, Research Center for Photovoltaics, Tsukuba, Ibaraki, Japan

[b]National Institute of Advanced Industrial Science and Technology, Fukushima Renewable Energy Institute, Koriyama, Fukushima, Japan

Abstract. The properties of luminescence coupling (LC) in multijunction solar cells were investigated in three-terminal InGaP//InGaAsP and InGaP/GaAs//InGaAsP tandem solar cells fabricated using the bonding technique through metal nanoparticle (MNP) arrays, where // denotes the mechanical stacking using MNP arrays. Power extraction in the three-terminal tandem solar cells is evaluated, showing that the power extraction in the devices is equivalent to a sum of the power extraction of the top and bottom subcells. In addition, the properties of the LC effect are investigated in the three-terminal tandem devices. The LC current increases with the illuminated light intensity and shows a bias-voltage dependency of the subcell that is emitting luminescence. We also discuss the impact of LC on the power extraction of the three-terminal tandem solar cells. [DOI: 10.1117/1.JPE.8.045503]

Keywords: luminescence coupling; three-terminal tandem solar cells; multijunction solar cell; luminescence.

Paper 18130 received Nov. 3, 2018; accepted for publication Dec. 10, 2018; published online Dec. 22, 2018.

1 Introduction

Multijunction solar cells composed from different bandgap semiconductors have achieved higher efficiency compared with conventional single-junction solar cells.[1,2] Dual-junction III–V//Si devices with mechanically stacked, independently operated III–V and Si cells reach cumulative one-sun efficiencies over 30%.[3] The efficiency of two-terminal multijunction devices composed of series-connected subcells is easily reduced by a change in spectral irradiance because the current flow is strictly limited by the minimal current among the subcells. In contrast, in a parallel-connected, four-terminal, mechanically stacked tandem solar cell, subcells are electrically independent.[4] The four-terminal configuration thus has a distinctive advantage in yield potential, which, for example, is over 20% more than that for the two-terminal scheme device in Singapore.[5] The four-terminal tandem has the lowest levelized cost of electricity compared with the two-terminal tandem and single-junction solar cells.[6] In addition, the advantage of the four-terminal tandem solar cells is even more significant when we consider land scarcity, e.g., rooftop photovoltaic systems have limited space on vehicles and buildings.

Three-terminal tandem solar cells, developed by adding a third electrode into the two-terminal tandem solar cells, have also been considered as a plausible approach to maximize power extraction.[7] The three-terminal devices can adjust the current mismatching between the subcells and obtain robustness against the change of spectral irradiances. So far, the benefits of a three-terminal design have been investigated using device physics simulation. Although a previous study showed a slight increase in efficiency in three-terminal devices compared with that in four-terminal devices, owing to the reduced fill factor in four-terminal operation,[8] a performance equivalent to the four-terminal tandem solar cells is expected in general in three-terminal tandem

*Address all correspondence to Takeshi Tayagaki, E-mail: tayagaki-t@aist.go.jp

solar cells.[9] The three- and four-terminal tandem solar cells show higher efficiency than that of two-terminal devices for variable spectral irradiances.[10] In addition, three-terminal tandem solar cells with a back-contact-type bottom cell have been analyzed using model simulation.[11] Furthermore, three-terminal heterojunction bipolar transistor solar cell has been proposed, in which its detailed-balance efficiency limit was calculated and proved to be the same as that of a double-junction solar cell.[12]

In contrast to many model calculations, the literature is lacking in the experimental proof of three-terminal tandem solar cells. Monolithic three-terminal tandem solar cells have been fabricated by metalorganic chemical vapor deposition,[7,13] showing an active-area conversion efficiency of 19.9% in a three-terminal GaAs/Si configuration.[7] In addition, the integrated module of three-terminal devices using voltage matching circuit[14] can perform as well as the independent operation of the top and bottom cells.[15] The recent progress in wafer bonding[16] and mechanical stacking[17,18] has opened up new approaches for fabricating highly efficient three-terminal tandem solar cells with high crystal quality. These techniques can be transferred to develop three-terminal devices, which, however, have not yet been demonstrated to boost the energy yield for terrestrial use.

In our earlier studies, we have proposed a unique mechanical stacking technique using Pd nanoparticle (NP) arrays, named smart stack, which enables electrical and optical interconnections among dissimilar solar cells.[19,20] In addition, we have fabricated the InGaP/GaAs// InGaAsP/InGaAs solar cells,[19,21] InGaP/GaAs//Si solar cells,[22] and InGaP/GaAs/GaAs//Si solar cells,[23] where // denotes the mechanical stacking using metal NP (MNP) arrays. This bonding technique using Pd NP arrays leads to a low contact resistance ($\lesssim 1\ \Omega\,\mathrm{cm}^2$). In addition, even though the coverage of Pd NP is ~10% and a nanometer-sized air gap, with ~10-nm height, is formed between the subcells, a normal incident light can be transmitted with only ~2% absorption loss.[20] This may differ significantly from the mechanical stacking using conductive adhesives,[17] through which reflection occurs at the semiconductor/ITO interface because of the difference in refractive index. Furthermore, this bonding technique using Pd NP can stack the subcells of different sizes, providing area-mismatched multijunction devices.[24] Furthermore, pressing using low weight enables to stack the designed wafers without damaging the subcells. Thus, the smart stack can be used to fabricate the three-terminal tandem solar cells using various types of subcells, such as back-contact-type bottom cells.[11]

The three-terminal tandem solar cells are also useful for investigating the properties of luminescence coupling (LC). LC between subcells has been extensively studied in multijunction photovoltaic devices.[25–28] In tandem solar cells, luminescence in higher-bandgap subcells can be reabsorbed by the lower-bandgap subcells beneath. As LC facilitates in an increase in the photocurrent in the lower-bandgap subcell, it can improve the annual yield of tandem solar cells for terrestrial applications by increasing the tolerance against spectral mismatch when current mismatch due to spectral mismatch conditions is compensated for by the LC current generated in lower-bandgap subcells.[29] LC also affects the precise characterization, such as external quantum efficiency (EQE) measurements, of series-connected solar cells.[30] In addition, a previous study reported on the bias-voltage-dependent luminescence, where the LC efficiency may depend on the voltage applied to the device.[27,31] However, LC properties have not been well investigated from the viewpoint of the voltage dependence of a light-emitting subcell because in series-connected multijunction cells with two terminals, only the total output voltage can be measured, thus complicating the investigation of internal voltages in each subcell. Furthermore, the bias-voltage dependency of the LC may modify the maximum power conditions. In fact, if the luminescence in the higher-bandgap subcells can be enhanced by tuning the bias voltage applied to the subcell, the subcells would not be independently working in the three-terminal tandem solar cells.[8] The reabsorption of the luminescence leads to an increase in the photocurrent in the subcell, possibly increasing the voltage of the bottom subcell for the maximum power point (mpp). However, the impact of the coupling between subcells to the three-terminal tandem solar cells has not been understood well.

In this study, we fabricated mechanically stacked, three-terminal tandem solar cells through a bonding technique using MNP arrays. We then evaluated the power extraction in these three-terminal InGaP//InGaAsP and InGaP/GaAs//InGaAsP tandem solar cells. The power extraction of the tandem solar cells was compared with the individual subcell power extractions. In

addition, we investigated the properties of the LC effect in the three-terminal tandem solar cells. The LC current was measured using the three-terminal electrodes and showed an increase with an illuminated light intensity and a bias voltage of the subcell emitting luminescence. Finally, we discuss the LC effect on the power extraction of the three-terminal tandem solar cells.

2 Experimental

2.1 *Sample Preparation*

Three-terminal tandem solar cells were fabricated through a bonding technique using MNP arrays.[19] To investigate its fundamental properties, we used InGaAsP for the bottom subcells, in which better contact is easily obtained.[32] AuGeNi/Au and Ti/Au electrodes were formed in advance on the front and rear sides of the InGaAsP bottom cell using the electron-beam evaporation method [Fig. 1(a)]. An Au electrode was also formed in advance on the GaAs top cell with a thin GaAs contact layer. Figure 1(a) shows the top view of the devices. The centered square shows the top subcell with the top electrode, which is stacked at the center of the bottom subcell with two middle electrodes. The sizes of the top and InGaAsP bottom cells are $\sim 4.0 \times 4.0$ and $\sim 4.4 \times 8.0$ mm^2, respectively.

Figures 1(b) and 1(c) show a schematic of three-terminal InGaP//InGaAsP and InGaP/GaAs//InGaAsP tandem solar cells, respectively. The p–n junctions are bonded using Pd NP arrays to form a tandem solar cell comprising InGaP and InGaP/GaAs top cells and an InGaAsP bottom cell (1.15 eV) grown on an InP wafer. The fabrication processes follow the methods described in previous papers.[19,20] To form the Pd NP arrays, a diluted solution of polystyrene-*block*-poly-2-vinylpyridine was spin-coated on the surface of the bottom cell to form a nanometer-scale pattern. The bottom subcell with the middle and bottom electrodes was immersed in an aqueous solution containing Pd ions, and a patterned Pd template is formed on the bottom cell. Next, a plasma treatment was performed to remove the polymer and reduce the Pd ions to form the Pd NP arrays. The typical height of the Pd NPs and period of the arrays are ~10 and 100 nm, respectively. Next, the InGaP (InGaP/GaAs) top cell, which was grown on a GaAs wafer, was exfoliated using the epitaxial lift-off technique. The thin InGaP (InGaP/GaAs) top cell placed in water was then scooped up and transferred to the InGaAsP bottom cell, which is covered with Pd NP arrays. The stacked sample was pressed down using a weight at room temperature for 2 h. Finally, an SiO_2 and TiO_2 multistacked layer was formed as an antireflection coating on the front surface.

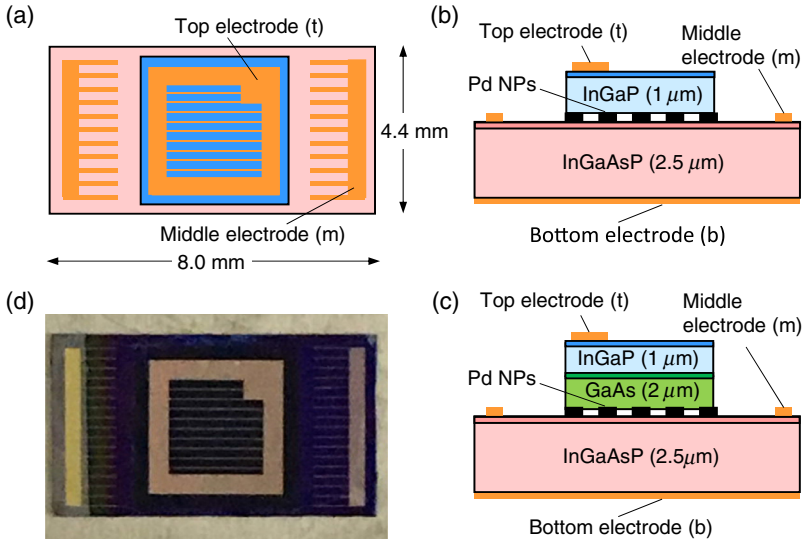

Fig. 1 (a) Top view of a three-terminal tandem solar cell. Side views of (b) the three-terminal InGaP//InGaAsP tandem solar cell and (c) InGaP/GaAs//InGaAsP tandem solar cells. (d) Digital camera image of a fabricated sample.

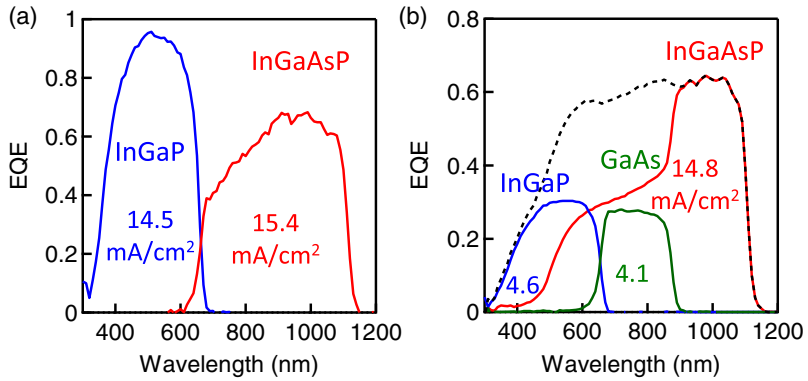

Fig. 2 EQE curves of the three-terminal (a) InGaP//InGaAsP and (b) InGaP/GaAs//InGaAsP tandem solar cells.

2.2 *Characterization of the Three-Terminal Tandem Solar Cells*

Current–voltage characteristics of the solar cells were measured using a Xe/halogen two-light-source solar simulator. EQE measurements of multijunction solar cells were performed by following the matured procedures for multijunction devices.[30] A modulated quasimonochromatic light combined with spectrally adaptable continuous bias light was used. The EQE was measured under a constant photon flux of 10^{14} photon/s/cm^2. In addition, the bias dependency of LC was evaluated from the current–voltage measurements conducted using a two-channel source meter (Keithley 2604B).

3 Results and Discussions

3.1 *Spectral Response of Subcells in Three-Terminal Tandem Solar Cells*

Figure 2(a) shows the EQE curves for the three-terminal InGaP//InGaAsP tandem solar cells. Here, we used a spatial mask to cover the surface of the bottom InGaAsP subcells to ensure equivalence in the illuminated areas of the top InGaP and bottom InGaAsP subcells. Although the InGaP subcell shows high EQE values, the InGaAsP subcell shows lower EQEs; this is partly caused by the interface reflection due to air gap at the bonded interface. Even though the EQE is reduced in the InGaAsP subcell, compared with the InGaP subcell, the InGaAsP subcell shows higher short-circuit current density (J_{sc}) implied by the EQE curve of 15.4 mA/cm^2.

Figure 2(b) shows the EQE curves for the three-terminal InGaP/GaAs//InGaAsP tandem solar cell. The device size is defined by the bottom subcell size (~0.35 cm^2) and a spatial mask is not used. Note that the device area even for the top subcell is defined by the bottom subcell size for EQE measurements. Owing to the smaller subcell sizes (~0.16 cm^2), lower implied J_{sc} of 4.6 and 4.1 mA/cm^2 are obtained for the InGaP and GaAs subcells, respectively, compared with the InGaAsP subcells of 14.8 mA/cm^2.

3.2 *Power Extraction in Three-Terminal Tandem Solar Cells*

The power extraction in the proposed three-terminal tandem solar cells was analyzed using a simple model calculation method. Figure 3 shows a schematic of the optoelectronic equivalent circuit of the three-terminal tandem solar cells. Here, we used a dual-junction solar cell with three-terminal electrodes. In the device used in this work, the EQE measurements show that the photocurrent generated in the bottom subcell is higher than that in the top subcell as shown in Fig. 2. Therefore, as an example, we considered the case where the photocurrent generated in the bottom subcell (subcell #2) is higher than that in the top subcell (subcell #1). While the power is primarily extracted using top (t) and bottom (b) electrodes as in conventional two-terminal tandem solar cells, the additional power generated in bottom subcell #2 due to the

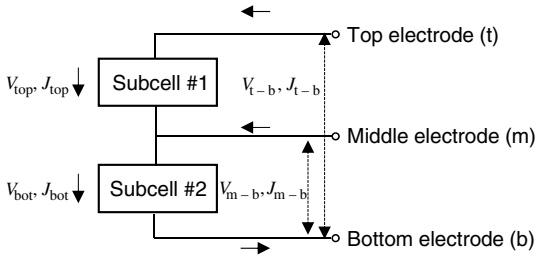

Fig. 3 Schematic of optoelectronic equivalent circuit of the three-terminal tandem solar cells.

current mismatch can be extracted using the middle (m) and bottom electrodes. The power extraction is determined by the product of voltage V_{t-b} (V_{m-b}) and current J_{t-b} (J_{m-b}) between the top (middle) and bottom electrodes as

$$P_{3T}[V_{top}, V_{bot}] = V_{t-b}J_{t-b} + V_{m-b}J_{m-b}. \tag{1}$$

Using the relations of $V_{t-b} = V_{top} + V_{bot}$, $J_{t-b} = J_{top}$, $V_{m-b} = V_{bot}$, and $J_{m-b} = J_{bot} - J_{top}$, where V_{top} (V_{bot}) and J_{top} (J_{bot}) are the voltage and current of the top (bottom) subcell, respectively, the power extraction is rewritten as

$$P_{3T}[V_{top}, V_{bot}] = (V_{top} + V_{bot})J_{top}[V_{bot}] + V_{bot}(J_{bot}[V_{bot}] - J_{top}[V_{top}]). \tag{2}$$

Finally, the power extraction is equivalent to the sum of the powers of top and bottom subcells:

$$P_{3T}[V_{top}, V_{bot}] = V_{top}J_{top}[V_{top}] + V_{bot}J_{bot}[V_{bot}]. \tag{3}$$

This indicates that the power extraction in the three-terminal device is equivalent to the sum of the power extraction of the subcells. In addition, the power extraction is maximized provided that the top and bottom subcells are at the maximum power condition ($V_{top,mpp}$, $V_{bot,mpp}$); this in turn implies that the power extraction in the three-terminal configuration is equivalent to the power extraction in the four-terminal tandem solar cells. Accordingly, the maximum power condition of the three-terminal tandem solar cells is determined as $V_{t-b,mpp} = V_{top,mpp} + V_{bot,mpp}$, and $V_{m-b,mpp} = V_{bot,mpp}$.

Next, we evaluated the power extraction in the fabricated devices. The current–voltage curves were measured with varying terminal conditions. Figure 4(a) shows the current–voltage curves of the three-terminal InGaP/InGaAsP tandem solar cells. First, the current–voltage curve for the bottom subcell was measured using middle–bottom electrodes, while the top electrode was set at an open-circuit condition. Then, the voltage of the maximum power condition, $V_{m-b,mpp}$, was determined from the current–voltage curve. Second, the current–voltage curve for the tandem solar cells was measured using the top–bottom electrodes, where the voltage between the middle

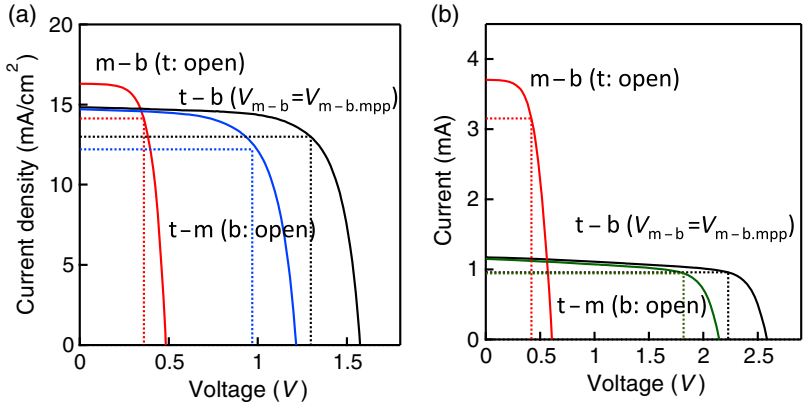

Fig. 4 Current–voltage curves of the three-terminal (a) InGaP//InGaAsP and (b) InGaP/GaAs//InGaAsP tandem solar cells.

and bottom electrodes was set at the maximum power condition $V_{m-b} = V_{bot,mpp}$. Then, the maximum power extraction and condition were determined from this curve as $P_{t-b,mpp}$, $V_{t-b,mpp}$, and $J_{t-b,mpp}$. Finally, the current of the middle–bottom electrodes at the maximum power condition of $J_{m-b,mpp}$ was measured under the condition that both the top–bottom and middle–bottom electrodes were set at voltages for the maximum power condition, i.e., $V_{m-b,mpp}$ and $V_{t-b,mpp}$, respectively. Based on the obtained voltages and currents for the maximum power condition, we determined the power extraction as $P_{3T} = P_{t-b,mpp} + P_{m-b,mpp} = 16.86 + 0.39 = 17.25\%$ for the InGaP//InGaAsP tandem solar cells. Note that the current difference between the top and bottom subcells is low, and thus the additional power extraction using the middle–bottom electrodes is low. For comparison, we determined the total power extraction using the maximum power extraction of each subcell, which in turn was determined by measuring the current–voltage curves when the unmeasured subcells were set at the open-circuit condition. The value was obtained as $P_{4T} = P_{top} + P_{bot} = 12.20 + 5.09 = 17.29\%$, which is comparable to the aforementioned value obtained by the three-terminal electrodes (17.25%).

Next, we investigated the three-terminal InGaP/GaAs//InGaAsP tandem solar cells, which showed significant current mismatch between the InGaP/GaAs top cell and the InGaAsP bottom subcell owing to different cell sizes. Figure 4(b) shows the current–voltage curves of the three-terminal InGaP/GaAs//InGaAsP tandem solar cells. Here, a spatial mask is not used and the device size (~0.35 cm^2) differs from the area of the InGaP/GaAs top subcell (~0.16 cm^2). Therefore, the y axis represents the current. According to the same procedure as that used for the InGaP//InGaAsP tandem solar cell, the power extraction in the three-terminal InGaP/GaAs//InGaAsP tandem solar cells was determined as $P_{3T} = P_{t-b} + P_{m-b} = 2.134 + 1.013 = 3.147$ mW. The additional photocurrent in the bottom InGaAsP subcell was extracted through the middle–bottom electrode. The value is consistent with the value obtained in the four-terminal configuration: $P_{4T} = P_{top} + P_{bot} = 1.717 + 1.325 = 3.042$ mW.

3.3 *Luminescence Coupling in Three-Terminal Tandem Solar Cells*

Next, we investigated the properties of LC using the three-terminal tandem solar cell. First, we used InGaP//InGaAsP tandem solar cells. To avoid a direct illumination into the bottom InGaAsP subcell, a spatial mask covering the surface of the bottom InGaAsP subcells was used. The illuminated 405-nm laser was absorbed only by the top InGaP subcell. Then, a photocurrent was generated in the InGaAsP bottom cell because of the reabsorption of the luminescent originated from the InGaP top cell. We measured the current–voltage curves for the InGaAsP subcell using the middle–bottom electrodes. Figure 5(a) shows J_{sc} of the InGaAsP subcell as a function of 405-nm laser intensity. In addition, according to the ratio of the LC current to the photocurrent generated through illumination in the top InGaP subcell, the LC efficiency is defined as $J_{sc,bot}/J_{sc,top}$. The LC efficiency in the InGaP//InGaAsP tandem solar cell was evaluated as $\sim 10^{-4}$, as shown in Fig. 5(a). The low LC efficiency is probably caused by low radiative recombination rate in the InGaP top cell because the LC efficiency reflects the external radiative

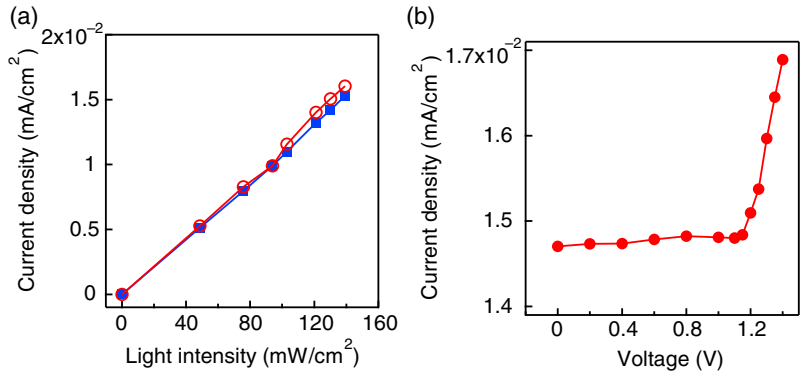

Fig. 5 (a) J_{sc} measured under the open-circuit (open circles) and short-circuit condition of the top–middle electrodes, as a function of the illumination intensity. (b) J_{sc} measured under light intensity of 140 mW/cm^2, as a function of the voltage applied to the top–middle electrodes.

efficiency of InGaP top cell η_{rad} and the transmittance of the luminescence at the top subcell into the bottom subcell, $t_{top \rightarrow bot}$, which is calculated to be an order of 10^{-1}.[33] Note that the LC efficiency depends on the properties of MNP arrays, such as the NP size. Compared with the adhesive bonding, the bonding technique using MNP forms a narrower gap between the subcells, which can provide a better LC efficiency.[33]

Here, the values of J_{sc} for the top electrode under the conditions of open- and short-circuit to the middle subcell were compared. Under the open-circuit condition, J_{sc} was determined to increase more with light intensity, compared with J_{sc} under the short-circuit condition. This indicates that the luminescence intensity at the InGaP top cell increases under the open-circuit condition. To understand this tendency, we measured the LC current for different bias voltages. Figure 5(b) shows J_{sc} as a function of the bias voltage. The current increases above 1.2 V, indicating enhanced luminescence in the InGaP subcells. Under a low bias-voltage condition, the photocarriers are partly recombined and emit light in the absorber before reaching the p–n junction owing to finite mobility. With increasing bias voltage, the photocarriers start to recombine at the p–n junction, and thus the radiative recombination at the junction leads to enhanced luminescence. This result is explained by the bias-voltage dependency of LC.[27]

Next, we measured the LC currents for 660- and 780-nm laser illuminations in the three-terminal InGaP/GaAs//InGaAsP tandem solar cells. Here, we used a spatial mask to cover the surface of the bottom InGaAsP subcells and investigated the coupling of the luminescence emitted from the GaAs subcell and reabsorbed by InGaAsP subcells. While the 750-nm laser was absorbed only by the GaAs subcell, the 660-nm laser was absorbed by both InGaP and GaAs subcells. Figure 6(a) shows the current–voltage curves for different 780-nm laser intensities under open- and short-circuit conditions of the illuminated top InGaP/GaAs subcell. Figure 6(b) shows J_{sc} as a function of light intensity under open- and short-circuit conditions. While the current increases with the laser intensity, a negligible difference was observed between the open- and short-circuit conditions. This can be understood by the unilluminated InGaP subcell, which prevents the current flow through the InGaP/GaAs subcell even under the

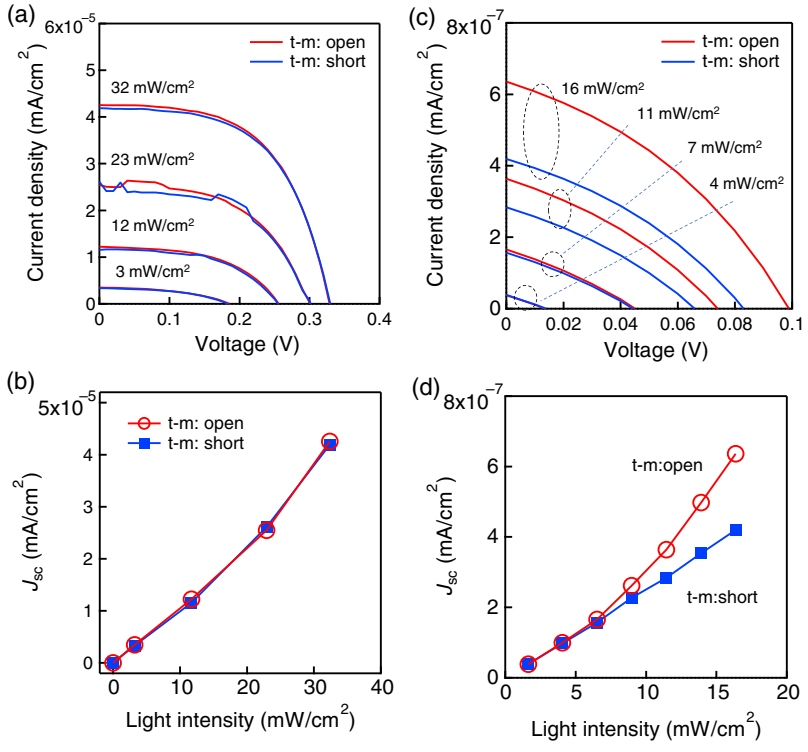

Fig. 6 (a) Current–voltage curves for different 780-nm laser intensities under open- and short-circuit conditions and (b) J_{sc} as a function of light intensity. (c) Current–voltage curves for different 660-nm laser intensities under open- and short-circuit conditions and (d) J_{sc} as a function of light intensity.

short-circuit condition. In addition, the LC efficiency of the InGaP/GaAs//InGaAsP tandem solar cells was estimated as $\sim 10^3$ for the luminescence from the GaAs to InGaAsP subcells.

Figure 6(c) shows the current–voltage curves for different 660-nm laser intensities under the open- and short-circuit conditions of the illuminated top GaInP/GaAs subcell. Figure 6(d) shows J_{sc} as a function of light intensity. While the LC current increases with the laser intensity, the current under the open-circuit condition shows higher current density than that under the short-circuit condition. This could be because both InGaP and GaAs subcells are illuminated by the 660-nm laser, thus enabling the current flow through the InGaP/GaAs subcell under the short-circuit condition. As a result, the photocarriers extracted as current increases, whereas the radiative carrier recombination decreases, resulting in reduced LC current under the short-circuit condition. This is consistent with the results that the LC current depends on the bias voltage applied to the subcell emitting luminescence, as shown in Fig. 5.

3.4 *Impact of the Coupling Between the Subcells to Power Extraction*

Finally, we discuss the impact of LC between the subcells on the power extraction in the three-terminal tandem solar cells. Although the LC of the devices used in this work is negligible, some devices show a significantly high LC efficiency.[26] The higher LC can modify the maximum power condition in the three-terminal tandem solar cells. As an example, we consider the power extraction of the three-terminal tandem solar cells with high LC efficiency. We used LC efficiency α defined as $J_{LC} = \alpha J_{0,top} \exp(qV_{top}/k_BT)$, where J_{LC} and $J_{0,top}$ are the LC current generated in the bottom subcell and the saturation current determining the dark current of the top subcell, respectively. The currents for the top and bottom subcells are given as

$$J_{top}[V_{top}] = J_{photo,top} - J_{0,top} \exp(qV_{top}/k_BT), \tag{4}$$

$$J_{bot}[V_{top}, V_{bot}] = J_{photo,bot} - J_{0,bot} \exp(qV_{bot}/k_BT) + aJ_{0,top} \exp(qV_{top}/k_BT), \tag{5}$$

where $J_{photo,top(bot)}$ and $J_{0,top(bot)}$ are the photocurrent and saturation current in the top (bottom) subcells, respectively. In contrast to the case of zero LC efficiency ($\alpha = 0$), the finite LC efficiency results in the enhanced power extraction of the bottom subcell by increasing the voltage of the top subcell. As a result, the optimum voltage of the top subcell increases more than the voltage under the maximum power condition with no LC current. Furthermore, in the top subcell, the current at the mpp decreases, and thus the current extracted from the middle–bottom electrodes increases owing to an increase in the LC current and reduced current extracted by the top–bottom electrodes. In practical devices, the subcell coupling is also caused by electronic properties, such as a low subcell shunt resistance.[30,31] Further studies on the impact of subcell couplings to the power extraction and its spectral robustness in three-terminal tandem solar cells are necessary.

4 Conclusion

We fabricated mechanically stacked, three-terminal tandem solar cells using MNP arrays. We evaluated the performances of the three-terminal InGaP//InGaAsP and InGaP/GaAs//InGaAsP tandem solar cells, showing that the power extraction in the three-terminal tandem solar cells is equivalent to those obtained in the devices with a four-terminal electrode configuration. In addition, we found that the LC current depends on the bias voltage of the subcell that is emitting luminescence, and it may modify the optimum power extraction condition in the three-terminal tandem solar cells.

Acknowledgments

A part of this work was supported by the New Energy and Industrial Technology Development Organization (NEDO) under the Ministry of Economy, Trade and Industry (METI) and KAKENHI (Grant No. 18K07987) from the Japan Society for the Promotion of Science.

References

1. R. M. France et al., "Quadruple-junction inverted metamorphic concentrator devices," *IEEE J. Photovoltaics* **5**(1), 432–437 (2015).
2. F. Dimroth et al., "Four-junction wafer-bonded concentrator solar cells," *IEEE J. Photovoltaics* **6**(1), 343–349 (2016).
3. S. Essig et al., "Raising the one-sun conversion efficiency of III–V/Si solar cells to 32.8% for two junctions and 35.9% for three junctions," *Nat. Energy* **2**, 17144 (2017).
4. M. Steiner et al., "Optically enhanced photon recycling in mechanically stacked multijunction solar cells," *IEEE J. Photovoltaics* **6**(1), 358–365 (2016).
5. H. Liu et al., "The realistic energy yield potential of GaAs-on-Si tandem solar cells: a theoretical case study," *Opt. Express* **23**(7), A382–A390 (2015).
6. S. Sofia et al., "Economic viability of thin-film tandem solar modules in the United States," *Nat. Energy* **3**(5), 387–394 (2018).
7. T. Soga et al., "High-efficiency monolithic three-terminal GaAs/Si tandem solar cells fabricated by metalorganic chemical vapor deposition," *Jpn. J. Appl. Phys.* **35**, 1401–1404 (1996).
8. E. L. Warren et al., "Maximizing tandem solar cell power extraction using a three-terminal design," *Sustainable Energy Fuels* **2**, 1141–1147 (2018).
9. M. Schnabel et al., "Equivalent performance in three-terminal and four-terminal tandem solar cells," *IEEE J. Photovoltaics* **8**(6), 1584–1589 (2018).
10. H. Schulte-Huxel et al., "Energy yield analysis of multiterminal Si-based tandem solar cells," *IEEE J. Photovoltaics* **8**(5), 1376–1383 (2018).
11. T. Nagashima et al., "Three-terminal tandem solar cells with a back-contact type bottom cell," in *Proc. 28th IEEE Photovoltaic Specialist Conf.*, pp. 1193–1196 (2000).
12. A. Martí and A. Luque, "Three-terminal heterojunction bipolar transistor solar cell for high-efficiency photovoltaic conversion," *Nat. Commun.* **6**, 7902 (2015).
13. M. Steiner et al., "A monolithic three-terminal GaInAsP/GaInAs tandem solar cell," *Prog. Photovoltaics Res. Appl.* **17**, 587–593 (2009).
14. J. M. Gee, "A comparison of different module configurations for multi-band-gap solar cells," *Solar Cells* **24**, 147–155 (1988).
15. M. Zehender et al., "Module interconnection for the three-terminal heterojunction bipolar transistor solar cell," *AIP Conf. Proc.* **2012**(1), 040013 (2018).
16. F. Dimroth et al., "Wafer bonded four-junction GaInP/GaAs//GaInAsP/GaInAs concentrator solar cells with 44.7% efficiency," *Prog. Photovoltaics Res. Appl.* **22**(1), 277 (2014).
17. A. C. Tamboli et al., "III-V/Si wafer bonding using transparent, conductive oxide interlayers," *Appl. Phys. Lett.* **106**, 263904 (2015).
18. C.-T. Lin et al., "Two-terminal metal-inter-connected multijunction III–V solar cells," *Prog. Photovoltaics Res. Appl.* **23**, 593–599 (2015).
19. H. Mizuno, K. Makita, and K. Matsubara, "Electrical and optical interconnection for mechanically stacked multi-junction solar cells mediated by metal nanoparticle arrays," *Appl. Phys. Lett.* **101**, 191111 (2012).
20. H. Mizuno et al., "Palladium nanoparticle array-mediated semiconductor bonding that enables high-efficiency multi-junction solar cells," *Jpn. J. Appl. Phys.* **55**, 025001 (2016).
21. T. Tayagaki et al., "Investigation of the open-circuit voltage in mechanically stacked InGaP/GaAs//InGaAsP/InGaAs solar cells," *Jpn. J. Appl. Phys.* **56**, 08MC01 (2017).
22. H. Mizuno et al., "High-efficiency III–V//Si tandem solar cells enabled by the Pd nanoparticle array-mediated 'smart stack' approach," *Appl. Phys. Express* **10**, 072301 (2017).
23. T. Sugaya et al., "Dual-junction GaAs solar cells and their application to smart stacked III-V//Si multijunction solar cells," *Appl. Phys. Express* **11**, 52301 (2018).
24. M. Baba et al., "Feasibility study of two-terminal tandem solar cells integrated with smart stack, areal current matching, and low concentration," *Prog. Photovoltaics Res. Appl.* **25**, 255–263 (2017).
25. M. A. Steiner and J. F. Geisz, "Non-linear luminescent coupling in series-connected multijunction solar cells," *Appl. Phys. Lett.* **100**(25), 251106 (2012).

26. A. Walker et al., "Impact of photon recycling and luminescence coupling in III–V photovoltaic devices," *J. Photonic Energy* **5**, 053087 (2015).
27. J. Jia et al., "Bias-dependence of luminescent coupling efficiency in multijunction solar cells," *Opt. Express* **23**(7), A219 (2015).
28. T. Tayagaki et al., "Transient analysis of luminescent coupling effects in multi-junction solar cells," *J. Appl. Phys.* **124**(19), 183103 (2018).
29. A. S. Brown and M. A. Green, "Radiative coupling as a means to reduce spectral mismatch in monolithic tandem solar cell stacks theoretical considerations," in *Proc. 29th IEEE Photovoltaic Specialist Conf.*, pp. 868–871 (2002).
30. M. Meusel et al., "Spectral response measurements of monolithic GaInP/Ga(In)As/Ge triple-junction solar cells: measurement artifacts and their explanation," *Prog. Photovoltaics Res. Appl.* **11**(8), 499–514 (2003).
31. D. Lan and M. A. Green, "Equivalent circuit analysis of radiative coupling in monolithic tandem solar cells," *Appl. Phys. Lett.* **106**(26), 263902 (2015).
32. T. Tayagaki et al., "Investigation of the properties of semiconductor wafer bonding in multijunction solar cells via metal-nanoparticle arrays," *J. Appl. Phys.* **122**, 023101 (2017).
33. T. Tayagaki et al., "Impact of nanometer air gaps on photon recycling in mechanically stacked multi-junction solar cells," *Opt. Express* (in press).

Biographies of the authors are not available.